

Geophysical Research Letters



RESEARCH LETTER

10.1029/2021GL093524

Key Points:

- 2-1/2 dimensional fully kinetic simulation of turbulent reconnection with a realistic, initially fluctuating magnetic field is performed
- Turbulent reconnection involving merging of macro-scale islands induces repeated micro-scale island formation in electron diffusion region
- During the macro-scale island merging, the micro-scale islands grow to larger scales, leading to an efficient cross-scale energy transfer

Supporting Information:

Supporting Information may be found in the online version of this article.

Correspondence to:

T. K. M. Nakamura,
takuma.tkm.nakamura@gmail.com









Citation:

Nakamura, T. K. M., Hasegawa, H., Genestreti, K. J., Denton, R. E., Phan, T. D., Stawarz, J. E., et al. (2021). Fast cross-scale energy transfer during turbulent magnetic reconnection. *Geophysical Research Letters*, *48*, e2021GL093524. <https://doi.org/10.1029/2021GL093524>

Received 27 MAR 2021

Accepted 9 JUN 2021

Fast Cross-Scale Energy Transfer During Turbulent Magnetic Reconnection

T. K. M. Nakamura^{1,2} , H. Hasegawa³ , K. J. Genestreti⁴ , R. E. Denton⁵ , T. D. Phan⁶ , J. E. Stawarz⁷ , R. Nakamura² , and W. D. Nystrom⁸ 

¹Institute of Physics, University of Graz, Graz, Austria, ²Space Research Institute, Austrian Academy of Sciences, Graz, Austria, ³Institute of Space and Astronautical Science, Japan Aerospace Exploration Agency, Sagami-hara, Japan, ⁴Southwest Research Institute, Durham, NH, USA, ⁵Department of Physics and Astronomy, Dartmouth College, Hanover, NH, USA, ⁶Space Sciences Laboratory, University of California, Berkeley, CA, USA, ⁷Department of Physics, Imperial College London, London, UK, ⁸Los Alamos National Laboratory, Los Alamos, NM, USA

Abstract Magnetic reconnection is a key fundamental process in collisionless plasmas that explosively converts magnetic energy to plasma kinetic and thermal energies through a change of magnetic field topology in a central electron-scale region called the electron diffusion region (EDR). Past simulations and observations demonstrated that this process causes efficient energy conversion through the formation of multiple macro-scale or micro-scale magnetic islands/flux ropes. However, the coupling of these phenomena on different spatiotemporal scales is still poorly understood. Here, based on a new large-scale fully kinetic simulation with a realistic, initially fluctuating magnetic field, we demonstrate that macro-scale evolution of turbulent reconnection involving merging of macro-scale islands induces repeated, quick formation of new electron-scale islands within the EDR which soon grow to larger scales. This process causes an efficient cross-scale energy transfer from electron- to larger-scales, and leads to strong electron energization within the growing islands.

Plain Language Summary Space above the Earth's atmosphere is broadly filled with ionized gas, called plasma. Since the density of the space plasma is mostly small enough to neglect the viscosity, the behavior of it is essentially different from neutral viscous fluids. In such a collisionless plasma system, the boundary layer between regions with different electromagnetic field and plasma properties plays a central role in transferring energy. One of the representative energy transfer processes in collisionless plasmas is magnetic reconnection that explosively converts magnetic energy to plasma kinetic energy through the topology change of magnetic field lines across the boundary layer with a large magnetic shear. On the other hand, understanding how the energy transfer between different spatiotemporal scales in turbulence, which has been commonly observed in space, is also a key for understanding the energy transfer physics in collisionless plasmas. In this study, based on a new plasma kinetic simulation of magnetic reconnection newly considering realistic, turbulent magnetic field fluctuations, it is found that during macro-scale evolution of the background fluctuations, the topology change of the reconnecting field lines occurs at multiple points within the micro-scale central region of reconnection. This process causes an efficient cross-scale energy transfer from micro- to larger-scales.

1. Introduction

In the Earth's magnetosphere, in situ spacecraft observations have directly confirmed many important signatures of magnetic reconnection with different spatiotemporal scales. Recently, high-time-resolution measurements by the Magnetospheric Multiscale (MMS) mission (Burch et al., 2016) successfully observed the electron diffusion region (EDR), resolving its electron-scale structures in the magnetotail for the first time on July 11, 2017 (Torbert et al., 2018). In this observation event, the EDR structures were nearly steady for a few seconds (~an ion gyro-period) during which the spacecraft crossed the EDR. Employing the high-performance fully kinetic simulation code VPIC (Bowers et al., 2008, 2009), our previous large-scale two-dimensional (2D) simulation of this event, in which the initial conditions were set based on the MMS data and a single reconnection point (X-line) was placed in a laminar state, successfully reproduced the steady EDR structures (T. K. M. Nakamura et al., 2018). Given the quantitative consistencies with the MMS data, the results further predicted that the normalized reconnection rate, which is a measure of the

© 2021. The Authors.

This is an open access article under the terms of the [Creative Commons Attribution License](https://creativecommons.org/licenses/by/4.0/), which permits use, distribution and reproduction in any medium, provided the original work is properly cited.

efficiency of the change in the magnetic field topology, was in the range $R \sim 0.15\text{--}0.2$ (Genestreti et al. 2018; T. K. M. Nakamura et al., 2018). As shown in Section 2.1, given mass and magnetic flux conservation near the EDR, it is predicted that the reconnection rate is roughly comparable to the aspect ratio of the EDR δ_e/L_e as $R \sim \alpha(\delta_e/L_e)$ (see Section 2.1 for derivation of this relation). Here $\alpha = B_{\text{in}}/B_0$ is the ratio between the magnetic field strength at the inflow-side edge of the ion diffusion region and in the upstream region. Indeed, the observed aspect ratio of this event ($\delta_e/L_e \sim 0.24 \pm 0.08$) was close to the reconnection rate (R. Nakamura et al., 2019). These previous results strongly suggested that formation of a steady EDR as seen in the laminar simulation really occurred in this MMS event.

However, MMS has observed a number of magnetotail reconnection events with more non-steady, turbulent features in field and plasma parameters (e.g., Ergun et al., 2018; Zhou et al., 2019). For example, on August 10, 2017, MMS observed stronger magnetic field fluctuations than those in the July-11 event with multiple V_{ix} (\sim ion outflow velocity) reversals, indicating the presence of multiple reconnection X-lines and/or strongly oscillating reconnection layers (Zhou et al., 2019). Substantial turbulent fluctuations accompanied by multiple flux rope encounters occurred even in the July-11 event after the EDR crossing interval (Stawarz et al., 2018; Teh et al., 2018). Past in situ observations have also shown that turbulent fluctuations in both field and plasma parameters commonly occur in the magnetotail (Angelopoulos et al., 1999; Borovsky et al., 1997; Neagu et al., 2002; Weygand et al., 2005), and that the fluctuations tend to be amplified in the magnetotail when the events are accompanied with bursty bulk flows (BBFs; Vörös et al., 2004) and auroral substorms (Stepanova et al., 2011), both of which are thought to be related to reconnection. These observational results strongly indicate that the magnetotail would commonly be in a turbulent state, and that turbulence can be enhanced by reconnection.

To investigate evolution and cross-scale interaction of turbulence, in this study, we perform an additional VPIC simulation with the same setting as the previous simulation of the July-11 event (T. K. M. Nakamura et al., 2018) except for the initial magnetic field perturbations. As described in Section 2, this new simulation employs a technique to set up an initially fluctuating magnetic field (T. K. M. Nakamura et al., 2020); an ensemble of k_x modes is added to the B_z (boundary normal) component to form a power-law spectrum with $-5/3$ scaling index for modes larger than the ion scales ($k_x d_i < 1$). The results show that the macro-scale evolution of turbulent reconnection involving merging of macro-scale magnetic islands induces repeated, quick formation of new secondary micro-scale islands within the EDR. As the merging of the macro-scale islands progresses, the micro-scale islands grow to larger scales, leading to an efficient cross-scale energy transfer from electron- to larger-scales.

2. Methods

2.1. Relation Between Reconnection Rate and Aspect Ratio of the Electron Diffusion Region

Based on the classic Sweet-Parker model of the ion diffusion region (Parker 1957; Sweet 1958), the conservations of mass and magnetic flux and the pressure balance between the upstream and downstream regions approximately give the following relation between the aspect ratio of the diffusion region and the normalized reconnection rate,

$$\frac{\delta}{L} \sim \frac{V_{\text{in}}}{V_{\text{out}}} \sim \frac{E_r}{V_A B_0} \left(\frac{B_0}{B_{\text{in}}} \right) \equiv R \left(\frac{B_0}{B_{\text{in}}} \right) \quad (1)$$

where L and δ are the width and thickness of the diffusion region, respectively, V_{in} and V_{out} are the inflow and outflow speed at the upstream and downstream edges of the diffusion region, respectively, V_A is the Alfvén speed, B_{in} is the magnetic field strength at the upstream edge, and E_r and $R \equiv E_r/V_A B_0$ are the unnormalized and normalized reconnection rates, respectively. Extending this relation to the inner EDR, the conservation of mass $V_{e,\text{in}} L_e \sim V_{e,\text{out}} \delta_e$ where L_e and δ_e are the width and thickness of the EDR, respectively, the pressure balance $B_{e,\text{in}}^2 / 2\mu_0 \sim m_e n V_{e,\text{out}}^2 / 2$ where $B_{e,\text{in}}$ is the magnetic field strength at the upstream edge of the EDR, and the flux conservation $E_r \sim V_{\text{in}} B_{\text{in}} \sim V_{e,\text{in}} B_{e,\text{in}}$ approximately give the aspect ratio of the EDR as,

$$\frac{\delta_e}{L_e} \sim \frac{V_{e,in}}{V_{e,out}} \sim \frac{V_{in}}{V_A} \left(\frac{B_{in}}{B_{e,in}} \right)^2 \sqrt{\frac{m_e}{m_i}} \sim \left(\frac{B_{in}}{B_{e,in}} \right)^2 \sqrt{\frac{m_e}{m_i}} \cdot \frac{\delta}{L} \quad (2)$$

Assuming a linear variation of the magnetic pressure in z ($B_{e,in} / B_{in}$)² $\sim (m_i / m_e)^{0.5}$, Equations 1 and 2 give,

$$\frac{\delta}{L} \sim \frac{\delta_e}{L_e} \sim R \left(\frac{B_0}{B_{in}} \right) \quad (3)$$

2.2. Simulation Settings

The simulation employed in this study was performed on the MareNostrum machine at the Barcelona Supercomputing Center, using the high-performance particle-in-cell code VPIC (Bowers et al., 2008, 2009), which solves the relativistic Vlasov-Maxwell system of equations. The initial simulation settings are the same as the ones employed in the study of T. K. M. Nakamura et al. (2018) to model an in situ observation of the steady EDR crossing by the MMS mission on July 11, 2017, except for the magnetic field perturbations that initiate reconnection. The simulation is 2-1/2 dimensional (2D variations in space with all three components of vectors) in the x - z plane. The initial magnetic field and number density are $B_x(z) = B_0 \tanh(z/L_0)$, $B_y = B_g$, and $n_{i,e}(z) = n_0 \text{sech}^2(z/L_0) + n_b$, where B_0 is the background reconnecting magnetic field component, B_g is the initial uniform guide field, n_0 is the Harris density component, n_b is the background density in the upstream region, and L_0 is the half-thickness of the initial current sheet. We obtained the initial magnetic field, density and temperature ratios from the MMS data as $B_g = 0.03B_0$, $n_0/n_b = 3.0$, $T_{i0}/T_{e0} = 3.0$, $T_{ib}/T_{eb} = 3.0$, and $T_{i0}/T_{ib} = T_{e0}/T_{eb} = 3.0$, where T_{i0} , T_{ib} , T_{e0} , and T_{eb} are the ion and electron Harris and background temperatures, respectively. L_0 is $0.6d_{i0}$, where d_{i0} is the ion inertial length based on n_0 . The ratio between the electron plasma frequency and the gyrofrequency is set to be $\omega_{pe}/\Omega_e = 2.0$. The ion-to-electron mass ratio is $m_i/m_e = 400$. The system size is $L_x \times L_z = 120d_{i0} \times 40d_{i0} = 2,400d_{e0} \times 800d_{e0} = 14,400 \times 4,800$ cells with a total of 1.4×10^{11} simulated particles, where d_{e0} is the electron inertial length based on n_0 . The boundary conditions are periodic along x , with conducting walls along z .

While T. K. M. Nakamura et al. (2018) added only one mode for the initial magnetic field perturbation with wavelength equal to L_x ($m_x = 1$) to initiate a single reconnection X-line, we investigate here the macro-scale turbulent evolution of multiple X-lines, by employing an ensemble of $m_x(k_x)$ modes in B_z to form a power-law spectrum with $-5/3$ slope at ion-inertial and larger scales ($k_x d_{i0} < 1$), as observed in the Earth's magnetotail during non-reconnection related intervals (Vörös et al., 2004). See T. K. M. Nakamura et al. (2020) for more details of the technique to set up an initially fluctuating magnetic field. As seen in the study of T. K. M. Nakamura et al. (2020), these initial magnetohydrodynamic (MHD)-scale modes inject energy to smaller scales and quickly form a spectral slope of the smaller-scale modes, which is smoothly connected to the MHD scales, sufficiently before the reconnection matures (see the black curve in Figure 1a).

3. Results

As the simulation proceeds, the amplitude of the initial perturbations is enhanced (Figure 1a), corresponding to the formation of multiple MHD-scale magnetic islands, as seen in Figure 1b. For these MHD-scale modes ($k_x d_i < 1$), as reconnection develops, the amplitude at larger scales gets stronger forming a ~ -2.7 slope near ion scales and shallower slopes at larger scales, which indicates energy being transferred to larger scales through the island merging process. Similar scaling indices near ion- and larger scales were seen in past kinetic simulations that had multiple island or flux rope evolution (Daughton et al., 2014; Franci et al., 2017) and a single X-line evolution (Adhikari et al., 2020). Past observations of the magnetic field fluctuations in the magnetotail also showed that similar scaling indices (~ -2.6 to ~ -1.6) were observed accompanied with BBFs (Vörös et al., 2004) and ion diffusion regions (Eastwood et al., 2009), while ~ -1.6 indices were observed for weaker non-reconnection associated fluctuations (Vörös et al., 2004). Accompanied by the enhancement of the MHD-scale modes, smaller-scale modes ($k_x d_i > 1$) are also amplified and form a sharper (~ -4) spectral slope, indicating the occurrence of a downward energy cascade from MHD-to-smaller

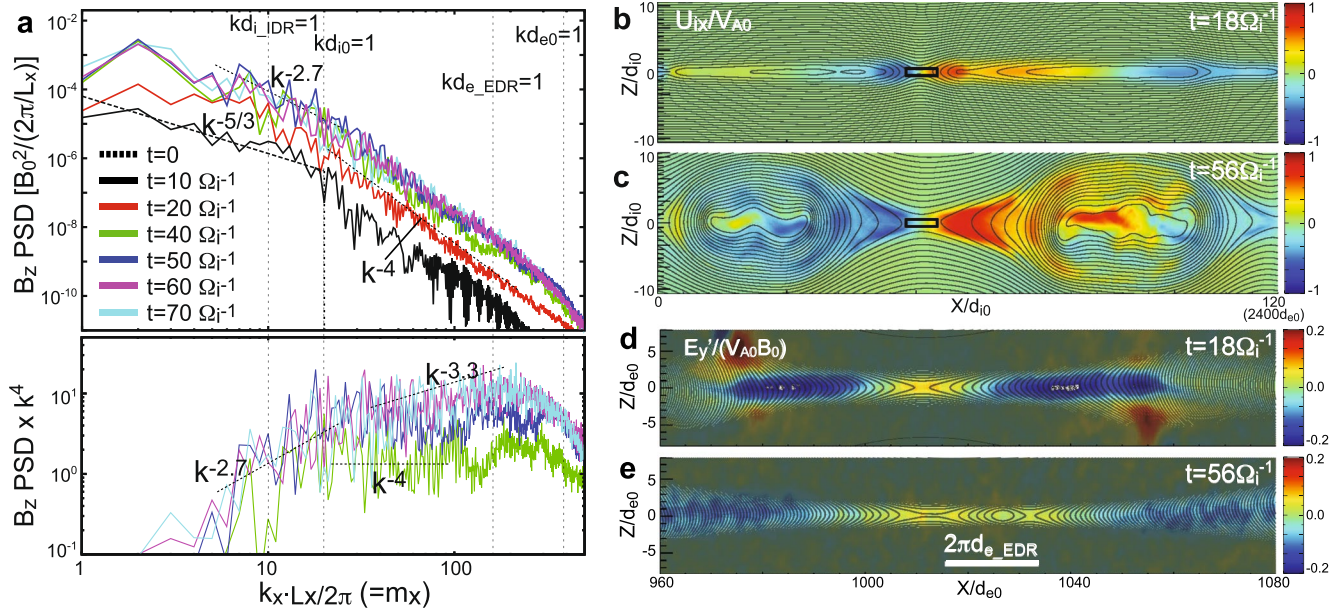


Figure 1. Multi-scale turbulent evolution of reconnection layer. (a) Time evolution of one-dimensional power spectra (k_x) of B_z modes averaged around the center of the current sheet ($Z = 0 \pm 2.5d_{i0}$), and the spectra multiplied by k_x^4 . Here, d_{i0} is the ion inertial length based on n_0 . The vertical dotted lines indicate the ion and electron inertial scales ($k_x d_i = 1$ and $k_x d_e = 1$) based on n_0 and the densities within the ion and electron diffusion regions n_{i_IDR} and n_{e_EDR} . (b–e) Color contours of U_{ix} with the magnetic field lines (b, c) and zoomed-in view of E_y' near the most developed X-line (marked by the black boxes in Figures 1b and 1c) (d, e) at $t = 18\Omega_i^{-1}$ and $t = 56\Omega_i^{-1}$. Here, $\Omega_i = eB_0 / m_i$ is the ion gyrofrequency based on the reconnecting magnetic field B_0 and \mathbf{E}' is the electric field in the electron frame $\mathbf{E}' = \mathbf{E} + \mathbf{U}_e \times \mathbf{B}$. The positive E_y' region surrounding the X-line is an indicator of the EDR (Zenitani et al., 2011).

scales (see black-to-red curves in Figure 1a). After reconnection matures ($t > 15\text{--}20\Omega_i^{-1}$), an additional peak is produced near electron scales, and the enhanced power of these modes spreads to larger scales with time (see green-to-cyan curves). This corresponds to an additional, repeated formation of electron-scale magnetized islands within the EDR (Figure 1e), which will be explained in detail in the next paragraphs.

As seen in Figures 2a and 2b, as the MHD-scale initial islands are merged into larger ones, the B_z peaks, where the reconnected field lines are most strongly piled-up, are transported farther away from the most developed X-line by the outflow jets. Here, notice that the B_z strength behind the peaks becomes smaller as the peaks move farther away from the X-line (Figure 2b). This occurs because the motion speed of the peaks ($dX_{\text{peak}}/dt > 0.2V_A$ as seen in Figure 3c) is almost always faster than the inflowing speed of the magnetic flux ($V_{\text{in}} \sim RV_A < 0.2V_A$ as seen in Figure 3d), resulting in the continuous decrease of the reconnected flux density behind the B_z peaks. As this flux density (i.e., B_z in the outflow region) decreases, it becomes more difficult for electrons to be magnetized in the outflow region, leading to the extension of the EDR in the x -direction (Daughton et al., 2006). Thus, as seen in Figure 2d, during the continuous MHD-scale island merging process, the aspect ratio of the EDR (δ_e/L_e) continuously decreases. Notice also that this δ_e/L_e decrease corresponds to the reduction of the reconnection rate as predicted in Equation 3 and shown in blue and red curves in Figure 2d. Here, δ_e and L_e are the vertical and horizontal lengths of the EDR defined as the positive E_y' region surrounding the most developed X-line, respectively. To remove the noise of the electric field data and better identify the location of the edge of the EDR where $E_y' = 0$, we used the 2D Gaussian smoothing filter near the edge of the EDR.

It is notable here that short time-scale ($\sim 1\Omega_i^{-1}$ or shorter) fluctuations are seen in the time variation of the reconnection rate after reconnection matures ($t > 15\text{--}20\Omega_i^{-1}$), and the amplitude of these fluctuations becomes larger as the rate itself decreases (Figures 2e and 2f). This corresponds to the repeated formation of the electron-scale islands within the EDR. Figure 3 shows this small-scale island evolution for a weak fluctuation interval at $t \sim 21.4\Omega_i^{-1}$ (blue-shaded interval in Figure 2e) and for a stronger fluctuation interval at $t \sim 56.0\Omega_i^{-1}$ (red-shaded interval in Figure 2f). At $t \sim 21.4\Omega_i^{-1}$, a small island whose length is less than the electron inertial-scale forms near the center of the EDR, but it quickly disappears in less than $0.2\text{--}0.4\Omega_i^{-1}$. On the other hand, at $t \sim 56\Omega_i^{-1}$, a larger island whose length is nearly close to $\lambda \sim 2\pi d_{e_EDR}$ forms. Here,

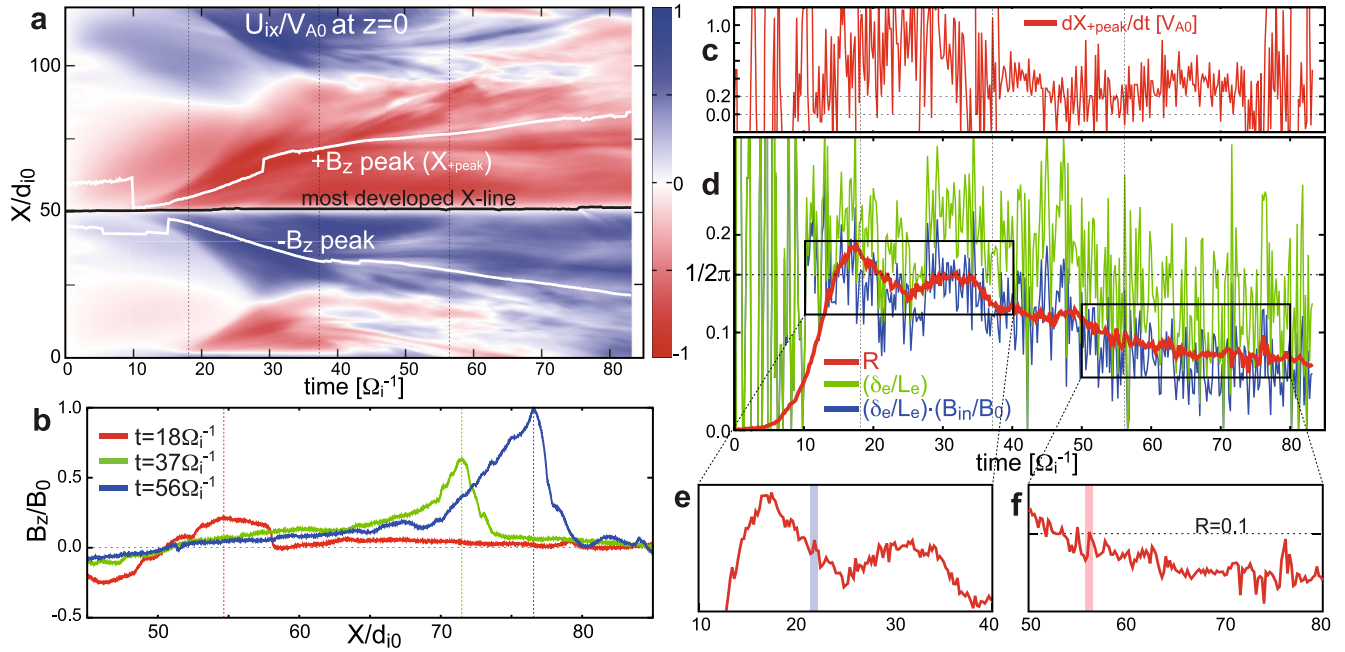


Figure 2. Evolution of reconnection rate and electron diffusion region (EDR) aspect ratio. (a) Time evolution of U_{ix} at $z = 0$ and the locations of the most developed X-line and the positive and negative B_z peaks. (b) Cuts at $z = 0$ of B_z at $t = 18\Omega_i^{-1}$, $t = 37\Omega_i^{-1}$, and $t = 56\Omega_i^{-1}$ (the times marked by dotted lines in Figure 2a). The vertical dotted lines mark the location of the positive B_z peak. (c, d) Time evolution of (c) the relative velocity of the positive B_z peak from the most developed X-line, and (d) the normalized reconnection rate R measured by the time derivative of the vector potential A_y at the most developed X-line (red), the aspect ratio of the EDR δ_e/L_e (green) and $(\delta_e/L_e)(B_{in}/B_0)$ (blue). B_{in} is the B_x magnitude at $(x, z) = (x_{X\text{-line}}, 0.5d_{i\text{-EDR}})$ where $x_{X\text{-line}}$ and $d_{i\text{-EDR}}$ are the x -coordinate of the most developed X-line and the ion inertial length based on the density within the ion diffusion region, respectively (corresponding to the edge of the ion diffusion region). (e, f) Zoomed-in views of the R evolution during the intervals marked by the black boxes in Figure 2d.

$d_{e\text{-EDR}}$ is the local electron inertial length based on density in the EDR, which roughly corresponds to the thickness of the EDR ($d_{e\text{-EDR}} \sim \delta_e$; Shay et al., 2001). This island propagates in the x -direction and is eventually absorbed into the region outside the EDR. The time scale of this island evolution within the EDR is $\sim 0.6\text{--}0.8\Omega_i^{-1}$.

Notice that the size of the island seen in Figures 3f–3i increases during its propagation, which corresponds to the energy transfer from electron- to larger scales and contributes to the formation of flatter spectra at small scales as seen in green-to-cyan curves in Figure 1a. Notice also that the island length at $t \sim 56\Omega_i^{-1}$ is close to the theoretically expected wavelength of the fastest growing mode of the electron tearing instability ($kl \sim 0.5$ where l is the half-thickness of the current sheet; Jain & Sharma, 2015). This indicates that as the EDR aspect ratio becomes smaller, larger islands, whose wavelength closer to the electron inertial scale ($\sim 2\pi d_{e\text{-EDR}}$), can grow more strongly within the EDR. Indeed, the visibly strong fluctuations of the reconnection rate (seen in Figures 2d–2f) occur when $\delta_e/L_e \sim d_{e\text{-EDR}}/L_e < 1/2\pi$.

The electron-scale magnetic island within the EDR has some unique features. Figure 4 shows a zoomed-in view near the electron-scale island at $t = 56\Omega_i^{-1}$. There is almost no enhancement of the core magnetic field (B_y) near the center of the island (Figure 4b), but a substantial enhancement of U_{ey} (Figure 4c) and a significant enhancement of the electron temperature (Figure 4d), which is mainly due to the enhancement of the out-of-plane component T_{ey} , are seen near the island center. These enhanced electron flow and temperature could be caused by electron acceleration by the positive E_y' , which is responsible for the conversion of the inflowing magnetic energy into particle energy (positive $\mathbf{J} \cdot \mathbf{E}' \sim J_y E_y'$) (Zenitani et al., 2011), filling the whole island including the O-point (island center) (see magenta curve in Figure 4e). Here, \mathbf{J} is the current density. Notice that the positive E_y' is seen within the whole island as long as the island stays within the EDR (see red-to-magenta curves), indicating that the magnetic energy is being dissipated not only near the X-line but also within the whole island as long as the island stays within the EDR. Consistently, the y -component of vector potential (A_y), which corresponds to magnetic flux surfaces, at both the X-line (the bottom of the curves) and the O-point (the positive peak near the X-line) decreases with time as seen in red-to-magenta

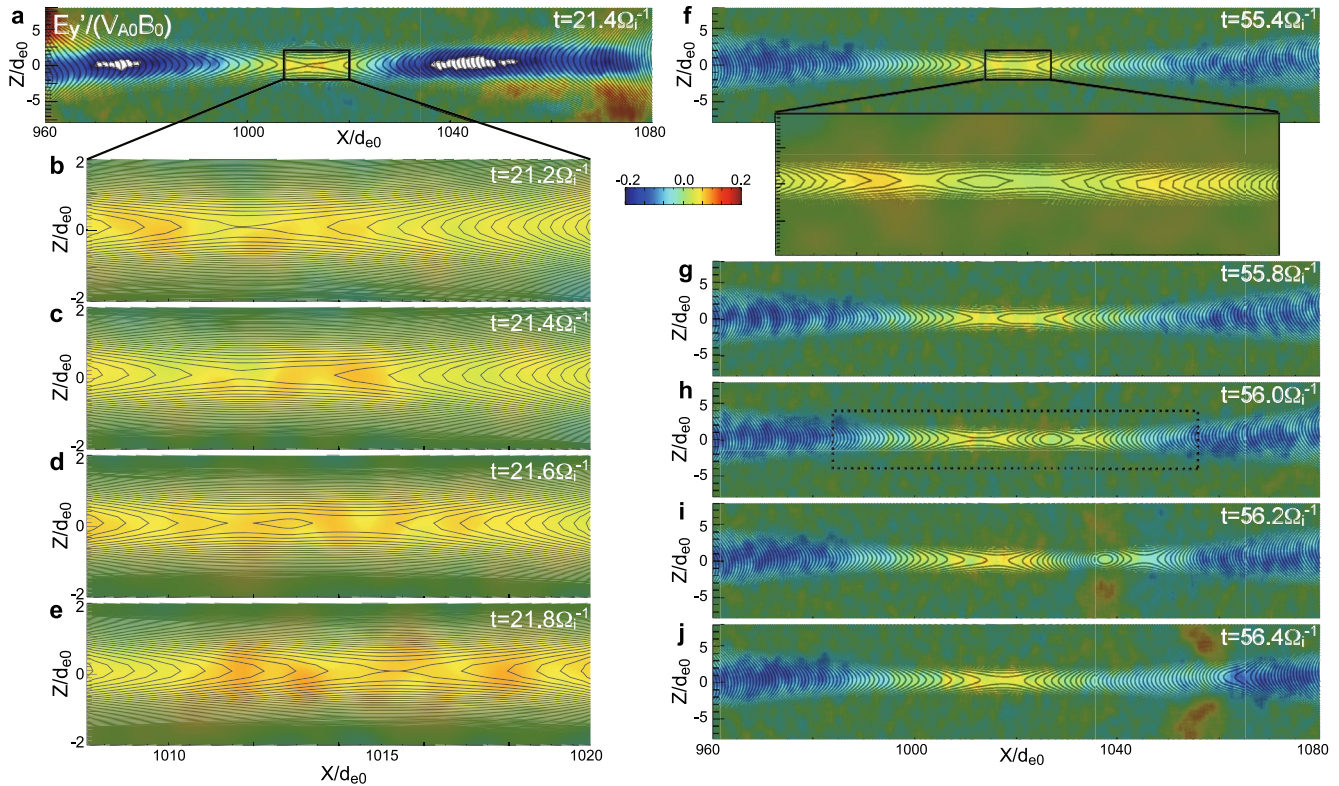


Figure 3. Evolution of micro-scale islands within extended electron diffusion region. Time evolution of zoomed-in views of E_y' , along with the magnetic field lines near the most developed X-line at the times around (a–e) $t = 21.4\Omega_i^{-1}$ and (f–j) $t = 56.0\Omega_i^{-1}$ (the time intervals marked by the blue- and red-shaded boxes in Figures 2e and 2f). The color ranges for all plots are the same as the ones in Figures 1d and 1e.

curves in Figure 4f. As the island propagates away from the EDR, the negative E_y' region appears within the EDR (i.e., a normal type island sandwiched between two positive E_y' regions is forming) as seen in Figure 4e. Correspondingly, the potential drop as well as the increase of T_{eyy} near the O-point cease as seen in cyan curves in Figures 4f and 4g.

4. Summary and Discussions

By both spatially and temporally resolving electron scales, we found repeated formation of spatially electron-scale islands within the EDR, whose lifetimes are comparable to or less than ion-scale. When MHD-scale turbulent fluctuations initially exist, as frequently observed in the Earth's magnetotail (Vörös et al., 2004), the merging of MHD-scale islands induced by the initial fluctuations not only amplifies the MHD-scale turbulence itself but also facilitates the micro-scale island evolution within the EDR. During the merging process, the faster transport of the piled-up reconnected flux relative to the flux inflow to the most developed X-line continuously reduces the flux density (B_z) in the outflow region, which makes it more difficult for outflowing electrons to be magnetized and leads to the continuous decrease of the EDR aspect ratio and the reconnection rate. This allows micro-scale islands to become larger within the EDR, leading to an additional energy transfer to larger scales.

A similar micro-scale island formation is seen even in the simulation of a single X-line (see the supporting information), although the transport of the piled-up flux and the resulting generation of larger islands can easily be inhibited once the outflow jets reach the periodic simulation boundaries. Past fully kinetic simulations of a single X-line with open simulation boundaries by Daughton et al. (2006) demonstrated larger island formations near the extended EDR, indicating the possibility of the cross-scale energy transfer even in the single X-line case, although they treated only on ion- or larger-scale island evolution. Thus, the

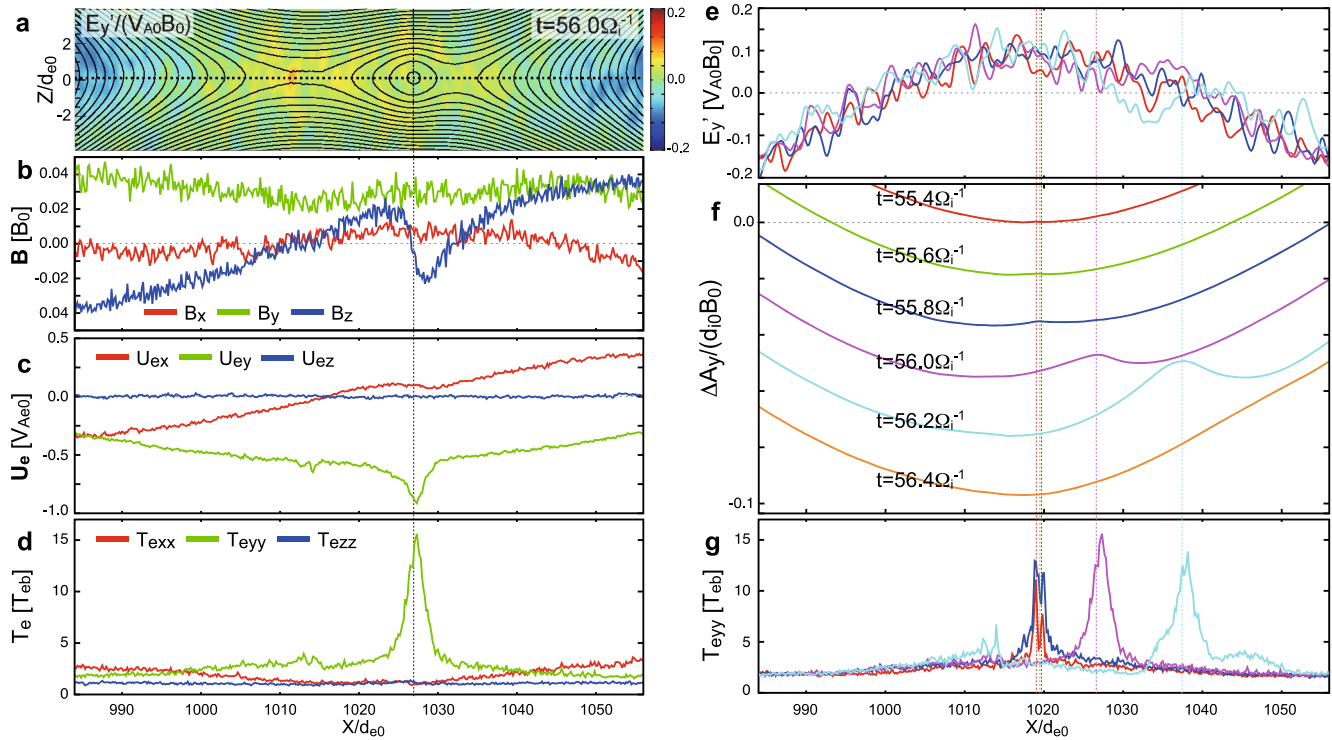


Figure 4. Structures of an electron-scale island within extended electron diffusion region. (a) Color contour with the magnetic field lines of E_y' in the region marked by the black box in Figure 3h at $t = 56.0\Omega_i^{-1}$. (b–d) Cuts along the black dotted line ($z = 0$) in Figure 4a of (b) the magnetic field components B_x , B_y , and B_z , (c) the electron bulk velocities U_{ex} , U_{ey} , and U_{ez} , and (d) the electron temperature components T_{exx} , T_{eyy} , and T_{ezz} . (e–g) Time evolution of the cut of (e) E_y' , (f) A_y , and (g) T_{eyy} along the same line in Figure 4a during $t = 55.4\text{--}56.4\Omega_i^{-1}$. The vertical dotted lines in Figures 4e–4g mark the O-point of the magnetic island at each time.

EDR structures would be commonly in a non-steady, turbulent state through the formation of micro-scale islands, and this can cause the additional cross-scale energy transfer as long as the fast transport of the reconnected flux occurs.

Note that in the present simulation, the initial fluctuations are added only for the MHD-scale modes, and as the simulation proceeds, subion- to electron-scale fluctuations with a spectral index ~ -4 spontaneously forms as seen in the black curve in Figure 1a. However, shallower spectral slopes at sub-ion- to electron scales were seen in some recent MMS observations in the magnetotail (e.g., Ergun et al., 2018). Since these small-scale fluctuations could be seed perturbations to induce magnetic islands within the EDR and control how quickly the islands grow, to understand the micro-scale island formation process within the actual EDR, it would be required to setup more realistic conditions for the initial turbulent spectra including the spectral slopes below subion scales.

Finally, since the present simulation further demonstrated that strong electron acceleration and heating occur when the island formed within the EDR becomes larger, these cross-scale and non-steady aspects of the EDR may significantly contribute to particle energization in reconnection. Further surveys considering 3D, asymmetries, and/or guide magnetic field effects would lead to a more comprehensive understanding of properties and roles of the non-steady EDR.

Data Availability Statement

The simulation data are available online via <http://doi.org/10.5281/zenodo.4641782>.

Acknowledgments

This work was supported by the Austrian Research Fund (FWF): P32175-N27. For the simulations employed in this study, the authors acknowledge PRACE for awarding us access to MareNostrum at the Barcelona Supercomputing Center (BSC), Spain. A part of the simulation data was analyzed with resources at the Space Research Institute of the Austrian Academy of Sciences. R. E. Denton was supported by NASA grant 80NSSC19K0254. J. E. Stawarz is funded by the Royal Society University Research Fellowship URF\R1\201286. The authors especially thank W. Daughton for their support to setup the VPIC simulations.

References

- Adhikari, S., Shay, M. A., Parashar, T. N., Sharma Pyakurel, P., Matthaeus, W. H., Godzieba, D., et al. (2020). Reconnection from a turbulence perspective. *Physics of Plasmas*, 27, 042305. <https://doi.org/10.1063/1.5128376>
- Angelopoulos, V., Mukai, T., & Kokubun, S. (1999). Evidence for intermittency in Earth's plasma sheet and implications for self-organized criticality. *Physics of Plasmas*, 6, 4161–4168. <https://doi.org/10.1063/1.873681>
- Borovsky, J. E., Elpic, R. C., Funsten, H. O., & Thomsen, M. F. (1997). The Earth's plasma sheet as a laboratory for flow turbulence in high- β MHD. *Journal of Plasma Physics*, 57, 1–34. <https://doi.org/10.1017/s0022377896005259>
- Bowers, K. J., Albright, B. J., Yin, L., Bergen, B., & Kwan, T. J. T. (2008). Ultrahigh performance three-dimensional electromagnetic relativistic kinetic plasma simulation. *Physics of Plasmas*, 15, 055703. <https://doi.org/10.1063/1.2840133>
- Bowers, K. J., Albright, B. J., Yin, L., Daughton, W., Roytershteyn, V., Bergen, B., & Kwan, T. J. T. (2009). Advances in petascale kinetic simulations with VPIC and Roadrunner. *Journal of Physics: Conference Series*, 180, 012055. <https://doi.org/10.1088/1742-6596/180/1/012055>
- Burch, J. L., Moore, T. E., Torbert, R. B., & Giles, B. L. (2016). Magnetospheric multiscale overview and science objectives. *Space Science Reviews*, 199, 5–21. <https://doi.org/10.1007/s11214-015-0164-9>
- Daughton, W., Nakamura, T. K. M., Karimabadi, H., Roytershteyn, V., & Loring, B. (2014). Computing the reconnection rate in turbulent kinetic layers by using electron mixing to identify topology. *Physics of Plasmas*, 21, 052307. <https://doi.org/10.1063/1.4875730>
- Daughton, W., Scudder, J., & Karimabadi, H. (2006). Fully kinetic simulations of undriven magnetic reconnection with open boundary conditions. *Physics of Plasmas*, 13, 072101. <https://doi.org/10.1063/1.2218817>
- Eastwood, J. P., Phan, T. D., Bale, S. D., & Tjulin, A. (2009). Observations of turbulence generated by magnetic reconnection. *Physical Review Letters*, 102, 035001. <https://doi.org/10.1103/physrevlett.102.035001>
- Ergun, R. E., Goodrich, K. A., Wilder, F. D., Ahmadi, N., Holmes, J. C., Eriksson, S., et al. (2018). Magnetic reconnection, turbulence, and particle acceleration: Observations in the Earth's magnetotail. *Geophysical Research Letters*, 45, 3338–3347. <https://doi.org/10.1002/2018GL076993>
- Franci, L., Silvio, S. C., Francesco, C., Landi, S., Papini, E., Verdini, A., et al. (2017). Magnetic reconnection as a driver for a sub-ion-scale cascade in plasma turbulence. *The Astrophysical Journal*, 850(1), L16. <https://doi.org/10.3847/2041-8213/aa93fb>
- Genestreti, K. J., Nakamura, T. K. M., Nakamura, R., Denton, R. E., Torbert, R. B., Burch, J. L., et al. (2018). How accurately can we measure the reconnection rate E_M for the MMS diffusion region event of 11 July 2017? *Journal of Geophysical Research*, 123, 9130–9149. <https://doi.org/10.1029/2018JA025711>
- Jain, N., & Sharma, A. S. (2015). Evolution of electron current sheets in collisionless magnetic reconnection. *Physics of Plasmas*, 22, 102110. <https://doi.org/10.1063/1.4933120>
- Nakamura, R., Genestreti, K. J., Nakamura, T. K. M., Baumjohann, W., Varsani, A., Nagai, T., et al. (2019). Structure of the current sheet in the 11 July 2017 electron diffusion region event. *Journal of Geophysical Research*, 124, 1173–1186. <https://doi.org/10.1029/2018JA026028>
- Nakamura, T. K. M., Genestreti, K. J., Liu, Y.-H., Nakamura, R., Teh, W.-L., Hasegawa, H., et al. (2018). Measurement of the magnetic reconnection rate in the Earth's magnetotail. *Journal of Geophysical Research*, 123, 9150–9168. <https://doi.org/10.1029/2018JA025711.1029/2018ja025713>
- Nakamura, T. K. M., Stawarz, J. E., Hasegawa, H., Narita, Y., Franci, L., Wilder, F. D., et al. (2020). Effects of fluctuating magnetic field on the growth of the Kelvin-Helmholtz instability at the Earth's magnetopause. *Journal of Geophysical Research: Space Physics*, 125, e2019JA027515. <https://doi.org/10.1029/2019ja027515>
- Neagu, E., Borovsky, J. E., Thomsen, M. F., Gary, S. P., Baumjohann, W., & Treumann, R. A. (2002). Statistical survey of magnetic field and ion velocity fluctuations in the near-Earth plasma sheet: Active Magnetospheric Particle Trace Explorers/Ion Release Module (AMPTE/IRM) measurements. *Journal of Geophysical Research*, 107(A7), 1098. <https://doi.org/10.1029/2001JA000318>
- Parker, E. N. (1957). Sweet's mechanism for merging magnetic fields in conducting fluids. *Journal of Geophysical Research*, 62, 509–520. <https://doi.org/10.1029/JZ062i004p00509>
- Shay, M. A., Drake, J. F., Rogers, B. N., & Denton, R. E. (2001). Alfvénic collisionless magnetic reconnection and the Hall term. *Journal of Geophysical Research*, 106, 3759–3772. <https://doi.org/10.1029/1999JA001007>
- Stawarz, J. E., Eastwood, J. P., Genestreti, K. J., Nakamura, R., Ergun, R. E., Burgess, D., et al. (2018). Intense electric fields and electron-scale substructure within magnetotail flux ropes as revealed by the Magnetospheric Multiscale mission. *Geophysical Research Letters*, 45, 8783–8792. <https://doi.org/10.1029/2018GL079095>
- Stepanova, M., Pinto, V., Valdivia, J. A., & Antonova, E. E. (2011). Spatial distribution of the eddy diffusion coefficients in the plasma sheet during quiet time and substorms from THEMIS satellite data. *Journal of Geophysical Research*, 116, A00124. <https://doi.org/10.1029/2010ja015887>
- Sweet, P. A. (1958). The neutral point theory of solar flares. In B. Lehnert (Ed.), *Electromagnetic Phenomena in Cosmical Physics* (Vol. 6, pp. 123–134). Cambridge University Press. <https://doi.org/10.1017/s0074180900237704>
- Teh, W., Nakamura, T., Nakamura, R., & Umeda, T. (2018). Oblique ion-scale magnetotail flux ropes generated by secondary tearing modes. *Journal of Geophysical Research: Space Physics*, 123, 8122–8130. <https://doi.org/10.1029/2018JA025775>
- Torbert, R. B., Burch, J. L., Phan, T. D., Hesse, M., Argall, M. R., Shuster, J., et al. (2018). Electron-scale dynamics of the diffusion region during symmetric magnetic reconnection in space. *Science*, 363, 1391–1395. <https://doi.org/10.1126/science.aat2998>
- Vörös, Z., Baumjohann, W., Nakamura, R., Volwerk, M., Runov, A., Zhang, T. L., et al. (2004). Magnetic turbulence in the plasma sheet. *Journal of Geophysical Research*, 109, A11215. <https://doi.org/10.1029/2004JA010404>
- Weygand, J. M., Kivelson, M. G., Khurana, K. K., Schwarzl, H. K., Thompson, S. M., McPherron, R. L., et al. (2005). Plasma sheet turbulence observed by Cluster II. *Journal of Geophysical Research*, 110, A01205. <https://doi.org/10.1029/2004ja010581>
- Zenitani, S., Hesse, M., Klimas, A., & Kuznetsova, M. (2011). New measure of the dissipation region in collisionless magnetic reconnection. *Physical Review Letters*, 106, 195003. <https://doi.org/10.1103/PhysRevLett.106.195003>
- Zhou, M., Deng, X. H., Zhong, Z. H., Pang, Y., Tang, R. X., El-Alaoui, M., et al. (2019). Observations of an electron diffusion region in symmetric reconnection with weak guide field. *The Astrophysical Journal*, 870, 34. <https://doi.org/10.3847/1538-4357/aaf16f>